

ANATOMICAL BASIS FOR BIOPHYSICAL DIFFERENCES BETWEEN *PINUS NIGRA* AND *P. RESINOSA* (PINACEAE) LEAVES¹

ROGER D. MEICENHEIMER,^{2,4} DOUGLAS W. COFFIN,³ AND ERIC M. CHAPMAN²

²Department of Botany and ³Department of Paper and Chemical Engineering, Miami University, Oxford, Ohio 45056 USA

Differences in the flexibility of *Pinus nigra* and *P. resinosa* leaves can be used to discriminate these two similarly looking pine species from one another. When bent along the longitudinal axis, *P. resinosa* leaves snap, while *P. nigra* leaves appear flexible. This useful field test has had no known biophysical or anatomical explanation until now. Analysis of the first order mechanics of bending and buckling of the pine needles was used to elucidate any important anatomical differences between these two species that can account for their different biophysical behaviors when bent. Neither the cross section of the total leaf area nor the inner core area between the two species differed significantly. Differences in the pattern of cell wall thickening and lignification of the endodermal layer of the inner core of the leaves best explain the differences in bending behavior. Thus, subtle variation in anatomy can influence the biophysical properties of naturally occurring structures, which in turn could have important implications for the engineering of manufactured objects.

Key words: anatomy; biophysics; brittle; flexible; leaves; Pinaceae; *Pinus*; sandwich composite beams.

Pinus nigra Arnold, introduced to North America in 1759, is superficially similar to *Pinus resinosa* Ait., native to the upper Great Lakes region. Both species bear two long (10–16 cm) needles per fascicle, but these leaves differ in their biophysical properties as indicated by differences in their responses to bending. A single *Pinus nigra* leaf bent between ones fingers will bend without breaking, whereas *Pinus resinosa* subjected to the same test will fail with a clean break. This field test is a useful characteristic that can be used to help discriminate these two pine species from one another (Hardin et al., 2001), but an explanation for this difference in bending behavior has been lacking. Development of a clear understanding of why these two seemingly similar leaves have extremely different responses will lead to a better understanding of the influence of anatomical differences in tissue composition on the mechanical responses of biological structures.

Leaves of a variety of monocot species have been modeled as sandwich composite beams with fiber composite faces separated by a low density, parenchymatous foam core (*Lolium perenne*: Vincent, 1982; *Iris*: Gibson et al., 1988; *Juncus effuses*: Niklas, 1991; *Zea mays*: Moulia et al., 1994; Moulia and Fournier, 1997). Similar composite beam models have been developed for stems of *Arundo donax* (Spatz et al., 1997), *Equisetum* (Spatz et al., 1993, 1998; Speck et al., 1998; Spatz and Emanns, 2004), *Triticum* (Hamman et al., 2005; Wang et al., 2006), and *Miscanthus* (Kaack and Schwarz, 2001; Kaack et al., 2003). We apply similar concepts to explain the observed differences of the flexible nonbrittle nature of *P. nigra* and the brittle nature of *P. resinosa* leaves. The important concept gained from this study is an appreciation of how subtle differences in organization of the components of the material can result in vastly different responses of the composite structure.

The objective of this study was to investigate the anatomical properties that underlie the biophysical difference between the

leaves of these two pine species. The insights gained from this approach should advance our understanding of the efficiency of naturally occurring structures and may be useful for improving the engineering of manufactured structures in general.

MATERIALS AND METHODS

Specimen collection—Two-year-old branches were collected from 20- to 30-yr-old *Pinus nigra* and *P. resinosa* trees growing on the Miami University Oxford campus during the summer of 2001 and 2007. Leaves from these branches were taken to the laboratory for immediate processing. Additional samples of both species were obtained from similarly aged trees growing in the Michigan State University W. K. Kellogg Experimental Forest in October 2006 and transported in plastic zip-locked bags in an ice chest to Oxford, then stored at 4°C until further processing.

Tensile tests—Uni-axial tensile tests were conducted on a universal mechanical testing machine (Instron Model 3344, Norwood, Massachusetts USA). Samples were prepared by affixing the ends of a single leaf to 205 g/m² linerboard tabs using an elastomeric adhesive (Liquid Nails LN600, ICI Paints, Strongsville, Ohio, USA). Pneumatic grips with serrated edges were used to hold the specimens. The free-span length was 50.8 mm. The tensile tests were conducted at a constant extensional rate of 0.424 mm/s. The elongation and load were recorded as a function of time. The axial stiffness was calculated as the maximum slope of the load vs. elongation curve determined numerically from the raw data. The stretch was the strain at failure, and the tensile strength was the maximum load achieved in the test.

Leaf bending failure—Leaves were sequentially bent around wooden dowels of various diameters under a dissecting microscope to observe the individual characteristics of leaf failure for each species.

Scanning electron microscopy—Broken leaves were trimmed to 1 cm lengths, fixed with 1% aqueous OsO₄, dehydrated with a graded series of ethanol, critical point dried with CO₂ using a Samdri-780A critical point drier (Tousimis Research, Rockville, Maryland, USA), mounted on SEM stubs, then sputter-coated with gold using a Denton Vacuum Desk II sputter coater (Denton Vacuum, Moorestown, New Jersey, USA) for the scanning electron microscopy study of the break area using a JEOL JSM-840A SEM (JEOL, Tokyo, Japan).

Light microscopy—Transverse sections (20 μm thick) of fresh leaves were cut using a Series 1000 Vibratome (Technical Products International, St. Louis, Missouri, USA). The sections were stained with a 0.1% phloroglucinol acidulated ethanol solution for 30 min (Ruzin, 1999), then mounted in glycerin to

¹ Manuscript received 3 April 2008; revision accepted 9 July 2008.

The assistance of G. Kowalewski at the W.K. Kellogg Experiment Station is gratefully acknowledged.

⁴ Author for correspondence (e-mail: MeicenRD@MUOhio.edu)

observe lignified tissues with bright field microscopy. Additional sections stained with 0.5% Sudan 4 were mounted in glycerin for fluorescence microscopy observation with a Nikon e600 Eclipse microscope (Nikon Instruments, Melville, New York, USA) using a UV-2E/C DAPI cube (EX 330–380, DM 400, BA 435–485).

Image analysis—Image Pro 4.1 Image Analysis software (Media Cybernetics, Silver Spring, Maryland, USA) was used to quantify leaf anatomical characteristics from uncompressed TIFF digital images. Areas of interest corresponding to the outer rind tissue (epidermis and hypodermis [EP + H]); mesophyll (M); resin canals (RC); inner core tissue (endodermis + transfusion tissue + vascular bundles [IC]) were established for each cross section (Fig. 1A). Cross-sectional areas were measured for the total leaf and individual tissue regions.

Pixels corresponding to the characteristic pink/purple color reaction for lignin in the bright field images and white-blue autofluorescence in fluorescence images were thresholded. Percentage lignin in the outer rind (EP + H) and the inner core tissues (IC) was calculated as the ratio of thresholded pixels to total pixels for each tissue area.

Linear dimensions of leaf and tissue regions, indicated in Fig. 1B, used in a pine leaf model construction were also measured using Image Pro 4.1. Coordinates associated with these measurements were translated such that the origin for measurements corresponded to the abaxial vertex of each leaf cross section.

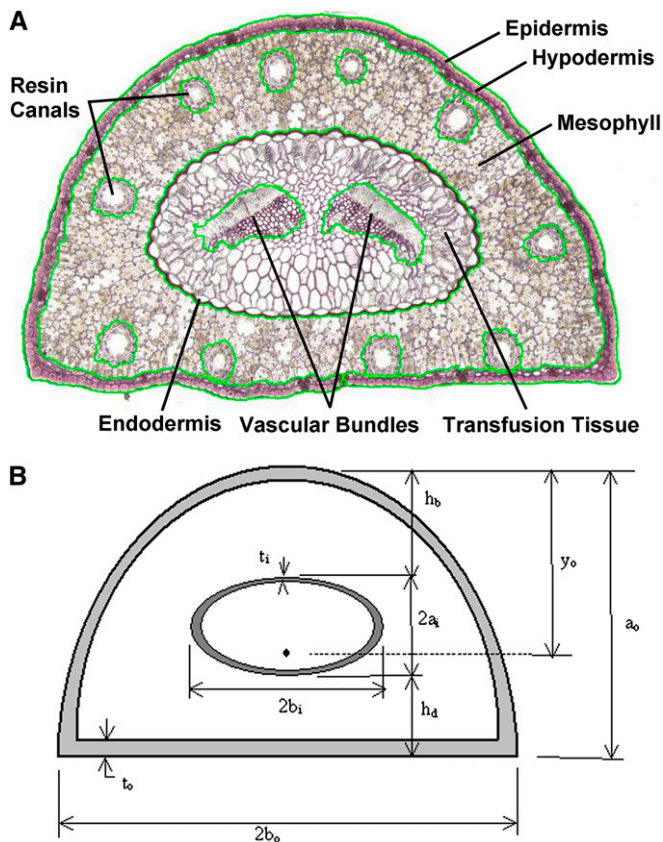


Fig. 1. Metric features measured from *Pinus* leaf cross sections. (A) Cross-sectional tissue areas demarked by green outlines are summarized in Table 3. Outer rind area includes epidermis + hypodermis. Inner core area includes endodermis + transfusion tissue + vascular bundles. (B) Measurements of tissue metrics used to construct idealized pine leaf model are summarized in Table 4. a_o = leaf height, $2b_o$ = leaf width, $2a_i$ = inner core height, $2b_i$ = inner core width, t_o = outer rind thickness, t_i = thickness of outer periclinal endodermis cell wall, h = length between outer walls of epidermis and endodermis, mesophyll thickness = $h - t_o$. Individual measurements were taken along the bisector running through the leaf vertex from both adaxial and abaxial halves of the leaves.

All individual measurements were entered in Microsoft (Redmond, Washington, USA) Excel spreadsheets and collated for statistical analysis. Student's t tests were used to establish statistical differences in measured parameters using Minitab Release 15 (Minitab Inc., State College, Pennsylvania, USA).

RESULTS

Leaf bending failure—When bent into freehand loops, *P. nigra* leaves had initial crimping failure on the flat adaxial side of the leaf (Fig. 2A–D). Under continued bending, the epidermis of the leaves ultimately broke in the vertical plane just interior to the adaxial corners of the leaves (Fig. 2E). Similar manipulation of *P. resinosa* leaves caused an abrupt failure of the leaf structure that was initiated at the vertex of the abaxial side of the leaf (Fig. 3A–D) and extended through the entire inner tissues of the leaf. After failure, the outer layer of the flat adaxial side of the leaf remained intact, but separated from the fractured interior tissues (Fig. 3E).

Pinus nigra bent around 68-mm dowels had no visible crimping when viewed with the dissecting microscope, but crimping occurred with dowels of 40 mm diameter or less at the 100% level and estimated to be about 50% failures at a diameter of 56 mm (Fig. 4, Table 1). *Pinus resinosa* had no failures when bent around dowels with a diameter of 23 mm, 100% failed at a diameter of 8 mm, and ~50% failed at a diameter of 13 mm (Fig. 5, Table 1).

Fracture surface comparison—The fracture surface of *P. nigra* formed an irregular boundary, whereas the fracture surface of *P. resinosa* was nearly orthogonal to the longitudinal leaf axis (Fig. 6). Elongated fibrous protrusions located primarily between the longitudinal stomatal rows extended beyond the fracture surface of *P. nigra*, whereas the fracture surface of *P. resinosa* was essentially devoid of these elements (Fig. 6).

Tensile tests—The tensile tests revealed that the response of the two species' leaves were quite different from each other (Fig. 7). *Pinus nigra* had a higher axial stiffness and a higher failure load, but a lower strain to failure than *P. resinosa* as indicated in Table 2. Based on the tensile response, *P. nigra* is more brittle than *P. resinosa*.

Leaf metrics and anatomy—Mean metrics for cross-sectional tissue areas and percentage lignification are summarized in Fig. 1A and Table 3. The mean linear metrics that were used to develop an idealized pine leaf model to explore the different biophysical behaviors of the two species leaves are summarized in Fig. 1B and Table 4.

There was no significant difference in the mean total cross-sectional areas of *P. nigra* and *P. resinosa* 2-yr-old leaves (TLA, Table 3). Difference in total leaf height (a_o , Fig. 1B) and total leaf width ($2b_o$, Fig. 1B) averaged 0.06 mm between the two species. Mean total leaf height was 0.04 mm shorter but mean total leaf width was 0.08 mm longer in *P. nigra* compared with *P. resinosa* (Table 4).

The mean area of the outer rind tissue (EP+H, Table 3) of *P. nigra* was significantly larger than that of *P. resinosa*. Mean thickness of the outer rind tissue of *P. nigra* was approximately twice that of *P. resinosa* on both the abaxial and adaxial sides of the leaves (t_o , Table 4). Percentage lignification of the outer rind of *P. resinosa* was significantly higher than that of *P. nigra* (%Lignin [EP+H], Table 3).

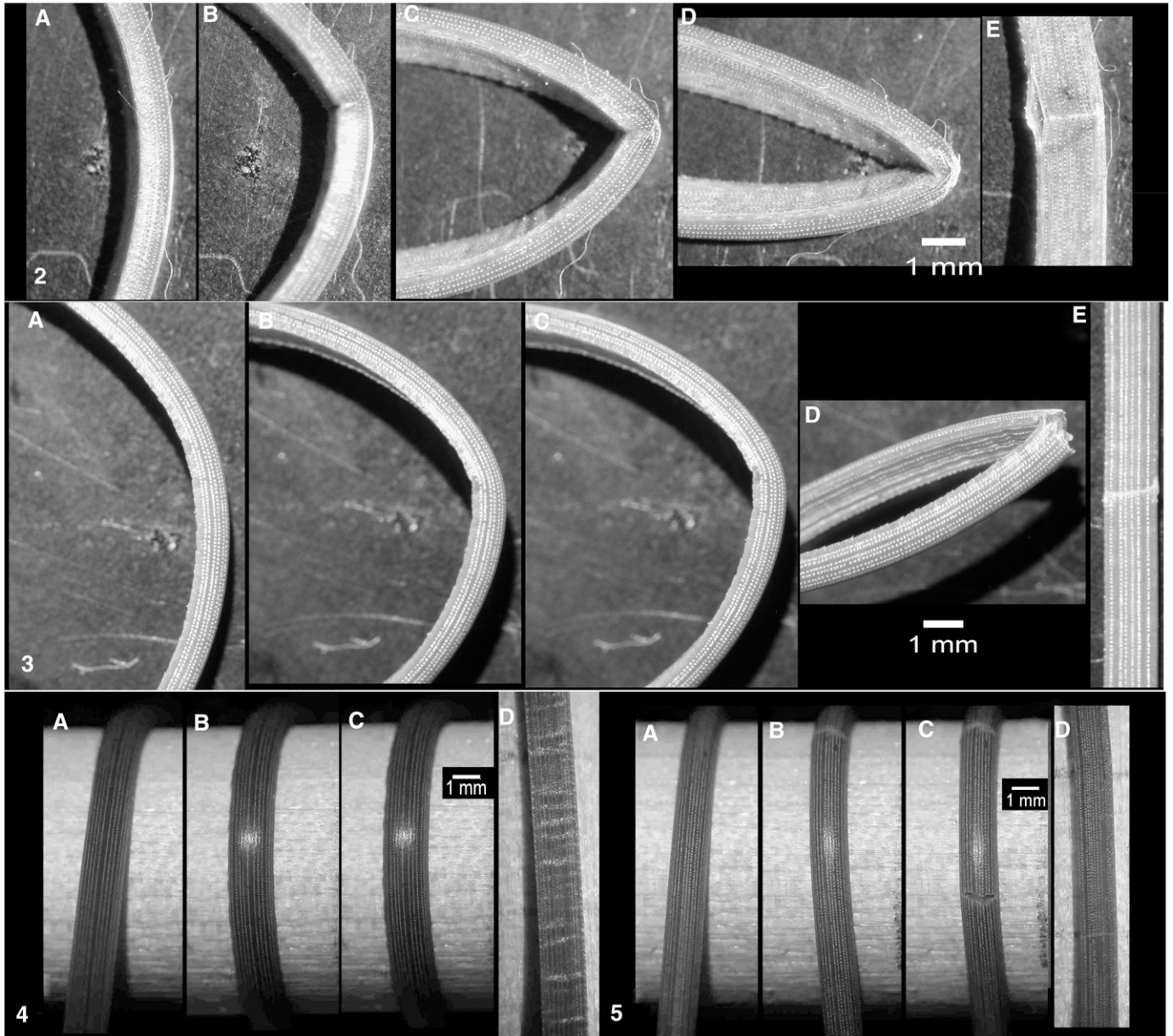


Fig. 2. *Pinus nigra* leaf at various stages of freehand bending toward flat adaxial surface. (A) No crimping visible. (B) Initiation of prominent crimp at adaxial edges. (C) Additional crimping along adaxial surface. (D) Failure at initial prominent crimp. (E) Adaxial surface of failed leaf illustrating longitudinal fracture and white transverse separation line of outer rind from intact inner tissues.

Fig. 3. *Pinus resinosa* leaf at various stages of freehand bending toward flat adaxial surface. (A–C) No crimping visible. (D) Abrupt failure initiates at vertex of abaxial leaf face and proceeds in an orthogonal plane toward adaxial surface. (E) Adaxial surface of failed leaf illustrating white transverse separation line corresponding with intact outer rind above fractured inner tissues.

Fig. 4. *Pinus nigra* leaf bent sequentially around a 10.8-mm dowel. Flat adaxial face of leaf is adjacent to dowel surface. Bending proceeds from top of image toward the bottom. (A) No visible crimping when bend is over 1/2 dowel diameter. (B) Crimping visible in upper half of leaf when bend is over 3/4 dowel diameter. (C) Crimping visible along entire leaf when bend is over entire dowel diameter. (D) Adaxial leaf surface after complete bend. White transverse lines correspond with regions that crimped at adaxial edges resulting in buckling of adaxial outer rind tissue away from inner leaf tissue.

Fig. 5. *Pinus resinosa* leaf bent sequentially around a 10.8-mm dowel. Flat adaxial face of leaf is adjacent to dowel surface. Bending proceeds from top of image toward the bottom. (A) No visible crimping when bend is over one-half the dowel diameter. (B) Initial failure at vertex of abaxial leaf face visible in upper half of leaf when bend is over three-fourths the dowel diameter. (C) Second failure at vertex of abaxial leaf face visible in midregion of leaf when bend is over entire dowel diameter. (D) Adaxial leaf surface after complete bend. Faint white transverse lines correspond with regions where fractured inner tissue intersects the intact adaxial outer rind tissue.

TABLE 1. Percentage failure of leaves in bending experiments. (A) *Pinus nigra* failed in compression; (B) *P. resinosa* failed in tension. $N = 20$ leaves per each dowel diameter.

Dowel diameter (mm)	Failure (%)
A) <i>P. nigra</i>	
93	10
67.5	10
52.5	40
42.6	20
38.5	100
28.3	100
B) <i>P. resinosa</i>	
28.3	0
22.8	0
15.6	20
12.6	55
10.8	65
7.7	100

Mean total mesophyll area (M), mean total resin canal area (RC), and mean total mesophyll minus resin canal area (M-RC) were all significantly larger in *P. resinosa* than in *P. nigra* leaves (Table 3). There was ~ 0.02 mm difference in mean

mesophyll thickness ($h-t_0$, Fig. 1B, Table 4) between the species. However, this difference was distributed differently between the two species, with *P. nigra* being thicker on the adaxial side and *P. resinosa* being thicker on the abaxial side of the leaf (mesophyll, Table 4). The abaxial mesophyll tissue was thicker than the adaxial mesophyll in both species, with a differential between the two sides of 0.07 mm for *P. nigra* and 0.1 mm for *P. resinosa*. The more numerous resin canals of *P. resinosa* were located closer to the surface of the leaves than were those of *P. nigra* (Fig. 8).

The mean area of the inner core tissues of the two species leaves were not significantly different (IC, Table 3). Mean inner core height ($2a_i$, Fig. 1B) was 0.04 mm shorter, but IC width ($2b_i$, Fig. 1B) was 0.1 mm longer in *P. nigra* compared with *P. resinosa* (Table 4). Within the inner core tissues, *P. nigra* had significantly more transfusion tissue area (TT), whereas *P. resinosa* had significantly more vascular bundle area (VB). The mean percentage lignification of *P. resinosa* IC was significantly greater than that of *P. nigra* (% lignin [IC], Table 3).

The endodermis enclosing the central transfusion tissue and vascular bundles of *P. nigra* had two regions of concave distortion in the abaxial and adaxial areas between the vascular bundles compared to the elliptical outline of the endodermis of *P. resinosa* (Fig. 8A, B). The thickness of the outermost periclinal cell wall of the endodermis (t , Fig. 1B) in *P. resinosa* was approximately twice that of *P. nigra* on both the adaxial and abaxial sides of the leaves (Table 4). Lignification of the endodermal cell was localized in adjacent anticlinal cell walls of *P. nigra* (Fig. 8A, C). Lignification of the *P. resinosa* endodermis was localized throughout the outermost periclinal cell walls (Fig. 8B, D).

DISCUSSION

The observed differences in the bending response of the leaves can be interpreted from differing points of view. On the surface, one might argue that because *P. resinosa* always breaks when tied into a knot, the leaf must be brittle and has high stiffness. The tensile results clearly contradict this argument; *P. resinosa* is significantly more ductile and has lower stiffness than *P. nigra*. Next, one could argue that *P. nigra* must be stronger than *P. resinosa*. Although true, the bending of the leaf with one's fingers is more akin to controlled deformation than that of an applied load. Therefore, *P. nigra* would require more load to bend the leaf, but failure would still be expected based on the curvature rather than the load level. Inspection of Figs. 2 and 3 reveal a more appealing explanation for the different responses. When the *P. nigra* is bent, the wall on the inside of the curvature collapses very early and a kink forms (Fig. 2B). This local buckling would reduce the tensile strain on the outer edges, thus avoiding tensile failure. Figure 3 shows that the leaf of *P. resinosa* has very little buckling on the inner edge. The maintenance of the cross-sectional integrity of the leaf of *P. resinosa* during bending causes high tensile strains on the outer edge, and thus, tensile failure occurs (Fig. 3D).

For tensile failure, as exhibited by *P. resinosa*, the failure could be explained to first order in terms of the maximum axial strain, which occurs at the outside face of the curved leaf. For bending into a radius of curvature, R , the axial strain, ϵ , is given as

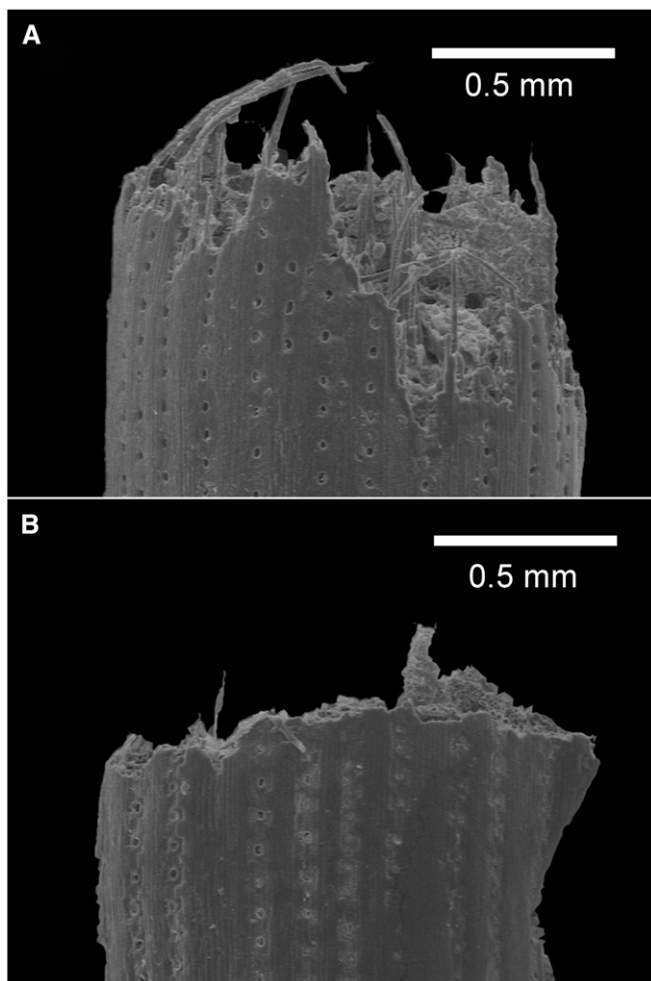


Fig. 6. Scanning electron micrographs of fracture surfaces of (A) *Pinus nigra* and (B) *P. resinosa* leaves after critical failure. Vertex of abaxial leaf face is in the central region for each leaf.

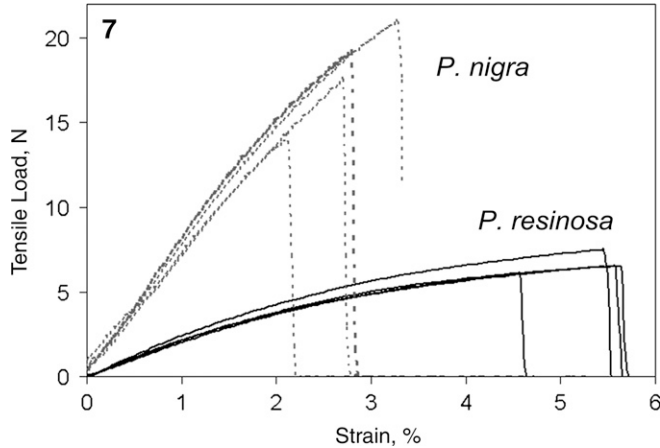


Fig. 7. Load–strain curves from axial tension tests for *Pinus nigra* (upper) and *P. resinosa* (lower) leaves. Load is the measured tensile load applied to the leaf. Strain is the measured elongation of the leaf divided by the original span length of 50.8 mm.

$$\epsilon = \frac{y}{R}, \tag{1}$$

where y is the distance from the neutral axis of the leaf. The maximum strain would be at the extreme faces of the leaf and be tension on the outer side and compression on the inner side. A prediction for tensile failure would be

$$R_{\text{tensile}} = \frac{y_o}{\epsilon_f}, \tag{2}$$

where y_o is given in Table 4 and ϵ_f is given in Table 2. Using the values for the parameters prescribed in Eq. 2 as given in Tables 2 and 4, one would expect tensile failure for *P. resinosa* at a radius of curvature of 10 mm. The bending results show, in fact, that a smaller radius of curvatures is achieved before tensile failure occurs with ~50% of the fibers that break at a radius of 6.5 mm. Based on Eq. 2, the smaller radius would correspond to a breaking strain of 8.2%. The observation that smaller radii of curvature are achieved than predicted by Eq. 2 is likely due to the fact that buckling on the inner side of the leaf will reduce the tensile strains on the outer edge and the location of the neutral axis would shift toward the tensile side. A shift of the neutral axis of 0.2 mm toward the tensile side would be required for Eq. 2 with a failure strain of 5.3% to predict failure at a radius of 6.5 mm.

TABLE 2. Mean and standard deviation of biophysical variables of *Pinus nigra* and *P. resinosa* leaves determined via tensile tests shown in Fig. 7. Axial stiffness was calculated as the maximum slope of the load vs. elongation curve determined numerically from the raw data. Tensile strength was the maximum load achieved in the test. ϵ_f = Strain at failure.

Variables	<i>P. nigra</i> (N = 4)	<i>P. resinosa</i> (N = 4)
Axial stiffness (N)	850 ± 60	260 ± 15
Tensile strength (N)	17.9 ± 3.0	6.7 ± 0.6
ϵ_f (%)	2.8	5.3

A secondary effect would be that local failure strains may be higher than those measured in the tensile test.

Although *P. nigra* does not undergo tension failure, Eq. 2 would predict that failure would occur with a radius of curvature of 20 mm or about twice that of the *P. resinosa*. With *P. nigra*, the buckling is severe, and the tensile strains are reduced to the point that breaking does not occur. A closer look at the local buckling is warranted. The buckling of thin-walled, linear-elastic and isotropic cylinders subjected to pure bending provides a prediction for the critical radius of curvature (R_{cr}) as (for example see Karamanos, 2002)

$$R_{cr} = 2.12 \frac{R^2 \sqrt{(1-\mu^2)}}{t}, \tag{3}$$

where t and R are the thickness and radius of the cylinder and μ is the Poisson ratio of the material. If one only considers that t is the thickness of the outer rind and takes R to be $a_0/2$ and $\mu = 0.3$, Eq. 3 predicts that *P. nigra* would fail in buckling at a radius of 8 mm and *P. resinosa* would fail at a radius of 14 mm. This prediction is contrary to the empirical observation that *P. nigra* fails in buckling before *P. resinosa*. Therefore, more than just the outer rind (epidermis and hypodermis) must play a role in explaining the biophysical differences between these species' leaves.

The second concern with this estimate using Eq. 3 is that the equation indicates that buckling should not occur at the radii observed for *P. nigra*. Figure 8 clearly shows that a cylinder is not a good representation of the cross sections of the leaves. The adaxial side is flat. Therefore, a better prediction may come from a local buckling model for a flat plate. The critical buckling load per unit length of plate (p_{cr}) for a long linear elastic and flat plate with width $2(b_0 - t_0)$ is given as

$$p_{cr} = \frac{\pi^2}{12} \frac{Et_0^3}{(1-\mu^2)(b_0 - t_0)^2}, \tag{4}$$

where E is the elastic modulus (Lekhnitskii, 1968). Assuming that the compressive load per unit length on the adaxial side is proportional to the strain from bending, the compressive load on the curved leaf can be written as

$$p_{cr} = \frac{Et}{R} (a_0 - y_o - \frac{1}{2}t_0), \tag{5}$$

where the geometric parameters are defined in Fig. 1B. Therefore, the critical radius of curvature can be expressed by equating Eqs. 4 and 5 to obtain

$$R_{cr} = \frac{12}{\pi^2} (1-\mu^2) (a_0 - y_c - \frac{1}{2}t_0) (\frac{b_0}{t_0} - 1)^2 \tag{6}$$

When $\mu = 0.3$, Eq. 6 predicts that $R_{cr} = 70$ mm for *P. nigra* and $R_{cr} = 200$ mm for *P. resinosa*. Eq. 6 shows that local buckling can indeed occur at large radii of curvature. Of course, buckling does not occur until much smaller radii of curvature because the inside of the leaf plays a role in resisting buckling. In fact, to reconcile the observations with predictions, the inside elements of the leaf must play a much larger role for *R. resinosa* in resisting buckling than for *P. nigra*.

TABLE 3. Mean (\pm SD) of anatomical tissue characteristics of 2-yr-old *Pinus nigra* and *P. resinosa* leaves. Data were analyzed for significance with Student *t* test.

Measurement	<i>P. nigra</i> (N = 9)	<i>P. resinosa</i> (N = 9)	t_{16}	P
TLA (mm ²)	1.148 \pm 0.043	1.157 \pm 0.010	-0.61	0.560
EP+H area (mm ²)	0.250 \pm 0.011	0.173 \pm 0.003	20.19	0.000 **
% Lignin (EP+H)	0.174 \pm 0.053	0.253 \pm 0.053	-3.18	0.006 **
M area (mm ²)	0.574 \pm 0.027	0.666 \pm 0.006	-9.97	0.000 **
TRC area (mm ²)	0.023 \pm 0.001	0.047 \pm 0.002	-33.16	0.000 **
M-RC area (mm ²)	0.551 \pm 0.027	0.619 \pm 0.006	-7.40	0.000 **
IC area (mm ²)	0.324 \pm 0.009	0.318 \pm 0.003	1.74	0.116
% Lignin (IC)	0.114 \pm 0.026	0.164 \pm 0.037	-3.34	0.005 **
TT area (mm ²)	0.267 \pm 0.010	0.255 \pm 0.007	2.81	0.014 *
VB area (mm ²)	0.057 \pm 0.005	0.063 \pm 0.006	-2.30	0.036 *

Notes: TLA = total leaf area, EP+H area = total outer rind (epidermis + hypodermis), % lignin (EP+H) = percentage lignification of outer rind, M area = mesophyll, TRC area = total resin canal, M-RC area = mesophyll-total resin canal, IC area = inner core (endodermis + transfusion tissue + vascular bundles), % lignin (IC) = percentage lignification of inner core, TT area = transfusion tissue, VB area = vascular bundle. Significance levels: * $\alpha < 0.05$; ** $\alpha < 0.01$.

Anatomical differences investigated through image analysis revealed that there was no significant difference in the total leaf cross-sectional areas of these two species of pine. *Pinus nigra* leaves had a notably thicker outer rind of lignified hypodermal fibers and epidermis. *Pinus resinosa* leaves had larger mesophyll cross-sectional area and more numerous resin canals, hence larger total resin canal area. There was no significant difference in the total inner core area of the leaves of the two species; however, *P. nigra* had more nonlignified transfusion

TABLE 4. Mean and standard deviation of empirical measurements of tissue metrics for *Pinus resinosa* and *P. nigra* leaves used to construct idealized pine leaf model as depicted in Fig. 1B. Data were analyzed for significance with Student's *t*-test.

Measurement	<i>P. nigra</i> (N = 8)	<i>P. resinosa</i> (N = 12)	t_{16}	P
a_0	0.956 \pm 0.022	0.996 \pm 0.008	4.52	0.004 **
b_0	0.779 \pm 0.015	0.744 \pm 0.003	6.05	0.001 **
y_0	0.533 \pm 0.017	0.538 \pm 0.029	0.44	0.664
a_i	0.230 \pm 0.005	0.252 \pm 0.002	10.87	0.000 **
b_i	0.450 \pm 0.014	0.396 \pm 0.002	9.74	0.000 **
y_i	0.530 \pm 0.017	0.536 \pm 0.029	0.57	0.575
t_{0b}	0.065 \pm 0.007	0.035 \pm 0.003	12.04	0.000 **
t_{0d}	0.057 \pm 0.004	0.036 \pm 0.004	10.73	0.000 **
t_{ib}	0.006 \pm 0.001	0.009 \pm 0.001	7.7	0.000 **
t_{id}	0.005 \pm 0.001	0.009 \pm 0.001	7.84	0.000 **
h_b	0.301 \pm 0.012	0.289 \pm 0.004	2.67	0.029 *
h_d	0.176 \pm 0.009	0.162 \pm 0.006	3.95	0.003 **
$(h_b - t_{0b})$	0.236 \pm 0.016	0.254 \pm 0.006	2.94	0.019 **
$(h_d - t_{0d})$	0.171 \pm 0.010	0.152 \pm 0.006	4.75	0.001 **

Notes: a_0 = leaf height, b_0 = half leaf width, y_0 = vertical distance of leaf centroid, a_i = half inner core height, b_i = half inner core width, y_i = vertical distance of inner core centroid, t_{0b} = abaxial outer rind thickness, t_{0d} = adaxial outer rind thickness, t_{ib} = thickness of abaxial outer periclinal endodermis cell wall, t_{id} = thickness of adaxial outer periclinal endodermis cell wall, h_b = abaxial length between outer walls of epidermis and endodermis, h_d = adaxial length between outer walls of epidermis and endodermis, $(h_b - t_{0b})$ = abaxial mesophyll thickness, $(h_d - t_{0d})$ = adaxial mesophyll thickness. Individual measurements were taken along the bisector running through the leaf vertex from both adaxial and abaxial halves of the leaves. All measurements in millimeters relative to vertex of leaves. Significance levels: * $\alpha < 0.05$; ** $\alpha < 0.01$.

tissue, whereas *P. resinosa* had more lignified vascular bundle tissue within this region. In addition, there were striking differences in the distribution of wall thickness and lignification patterns in the endodermal layer that formed the outer boundary of the IC (Fig. 8). In *P. nigra*, the thickness of the cell walls of the endodermis was uniform, and only the adjacent anticlinal cell walls of this cell layer were lignified. In *P. resinosa*, the outermost periclinal cell walls of the endodermis were twice as thick as the other walls, and lignification was observed throughout this thicker layer.

As noted by Niklas (1992), lignin functions as a bulking agent that can increase the compressive strength of cell walls. Fluorescence microscopy indicated that the mesophyll layer of *P. resinosa* (Fig. 8D) had relatively more lignified structure than *P. nigra* (Fig. 8C). This indicates that the mesophyll layer of *P. resinosa* would offer more resistance to local buckling of the outer rind than *P. nigra*. The lignification of the transfusion and mesophyll tissue would provide resistance to buckling of the outer wall. In addition, the lignified and thickened periclinal wall of the endodermis would offer much more resistance to compression than would the thin-walled periclinal cell walls of *P. nigra* endodermis. This internal difference in the structure of the endodermis is likely the cause for the main difference in bending behavior of the two leaves.

The internal structure of *P. resinosa* creates a sandwich construction for the leaf that has lignified inner and outer sheaths with a lignified inner core. Therefore, the effective bending stiffness will be sufficiently higher, and local buckling of the outer rind will occur at much lower radii of curvature than predicted by Eq. 6. For *P. nigra*, the inner core is composed of a thin-walled cell structure that would offer less resistance to buckling in compression. In addition, the core is likely to be more compressible, and thus, local buckling of the outer rind will occur sooner.

Another observed difference in the mechanical response of the needles is shown in the SEM images of broken leaves of *P. resinosa*; the leaves broke cleanly at the point of failure (Fig. 6B), while those of *P. nigra* tore irregularly along the leaf axis, which was associated with the elongated fibrous cells of the extensive hypodermis (Fig. 6A). Beismann et al. (2000) studied a number of *Salix* species that differed in the degree of brittleness of their twig bases. These workers concluded that there was no correlation between Young's modulus nor growth strains and the brittleness of twig bases. They did report that the "relative roughness" (ratio of rough area of fracture surface over the whole area of fracture surface) clearly corresponded with twig brittleness. In general, brittle twigs had smooth fracture surfaces, and nonbrittle species had rough fracture surfaces. While no correlation between absolute stress or strain and relative roughness was detected, there were good correlations between the ratio of stress or strain at yield over stress or strain at fracture ("index stress or strain") and relative roughness.

Speck and Spatz (2003) reported that brittle samples of *Arundo donax* (giant reed) rhizomes failed instantaneously when maximum stress was reached, creating a smooth fracture surface. Nonbrittle rhizomes had simultaneous partial fractures and were still capable of supporting loads after maximum stress levels were reached. The fracture surface of nonbrittle rhizomes had pronounced roughness.

Niklas (1992) noted that the total energy required to propagate a crack is the sum of the surface energy and the energy needed to produce plastic deformation. Beismann et al. (2000) observed that if the range of nonlinear behavior is negligible,

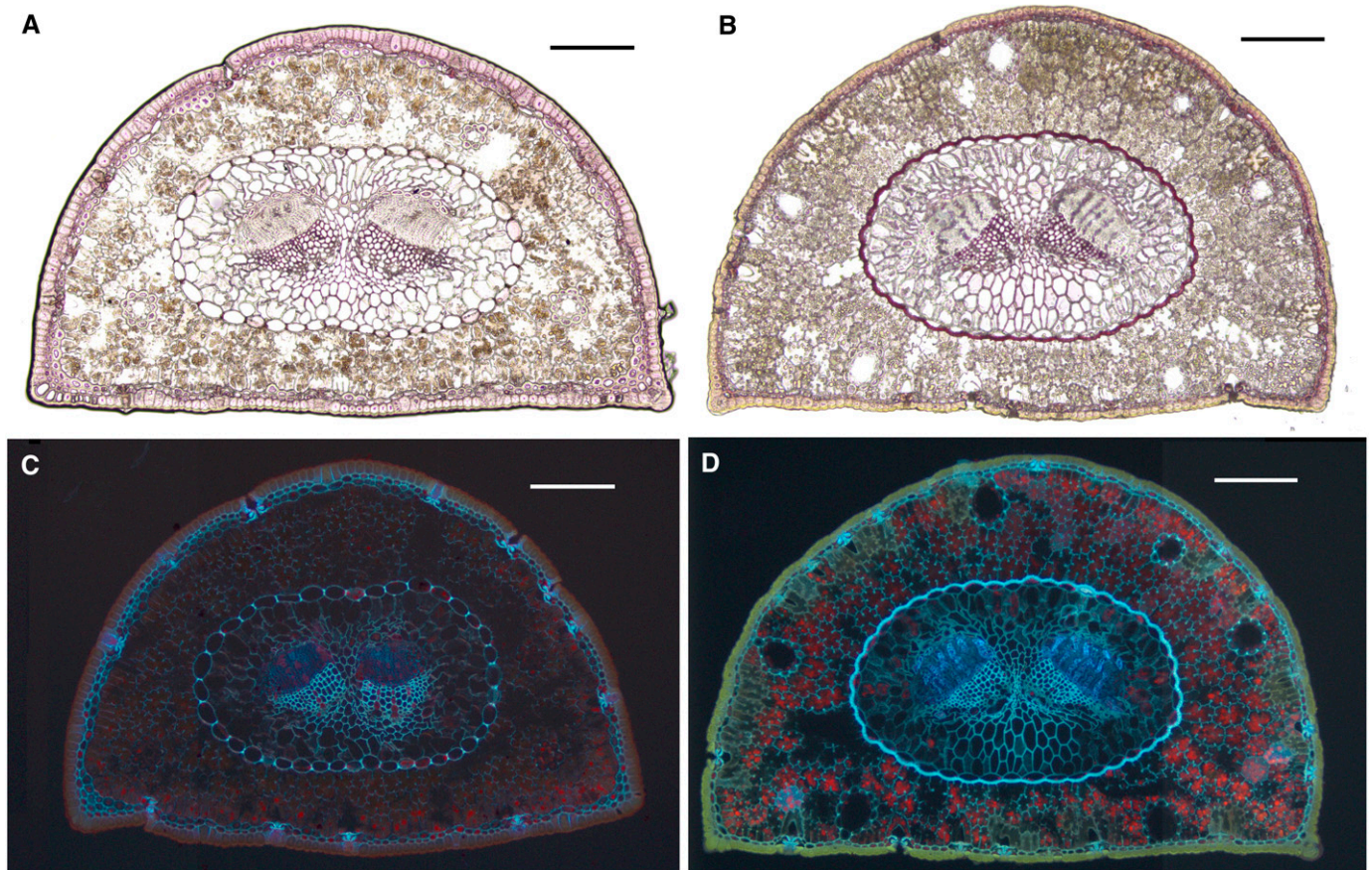


Fig. 8. Transverse sections of *Pinus* leaves. A, C. *Pinus nigra*. B, D. *Pinus resinosa*. (A, B) Bright field images stained with acidulated phloroglucinol to render lignified cell walls purple. (C, D) Fluorescence microscopy images of lignified cell walls with white-blue autofluorescence. Scales = 0.2 mm.

crack propagation requires predominately surface energy, but if nonlinear behavior dominates the force deflection curve, more energy is needed to propagate a crack, which results in a rough fracture surface with torn fibers.

The difference in fracture surfaces suggest that more energy is needed to break the elongated cells in *P. nigra* than to fracture the surfaces between cells, whereas in *P. resinosa*, the energy to break the cells is less than or equal to the energy needed to fracture between cells. The tensile tests showed that *P. nigra* was actually more brittle than *P. resinosa*, but buckled more easily. The observed fracture surfaces are in agreement with the conclusion that there is less structural integrity in *P. nigra*, which leads to buckling.

In conclusion, *Pinus resinosa* breaks when tied into a knot because the internal structure of the leaf provides rigidity that keeps the leaf's outer wall from buckling. The extent and location of the lignification in the leaf suggest that *P. resinosa* behaves as a sandwich structure. The resistance to buckling does not come only from the outer rind (epidermis + hypodermis) because the inner core (endodermis + transfusion layer + vascular bundles) adds significant structural rigidity to the leaf of *P. resinosa*.

Pinus nigra, on the other hand, can be tied into a knot without breaking because the leaf easily buckles during bending. Even though *P. nigra* has a thicker outer rind, the inner core of this species leaf offers less resistance to buckling. This lack of resistance appears to be related particularly

to the thin, nonlignified outermost cell wall layer of the endodermis, which appears to act more as an open-walled structure that does not offer buckling resistance. In addition, the relative lack of lignification in the IC and mesophyll tissues suggests lack of structural integration in the interior of this species leaf.

Despite the fact that in tension *P. nigra* is stronger and more brittle than *P. resinosa*, the lack of internal structure in *P. nigra* produces a fiber that is significantly more compliant in bending such that the field observations of bending leaves leads one to conclude that *P. resinosa* is the "brittle" fiber.

This research is an example of the initial phases in the "bottom-up" approach to biomimetics (Milwich et al., 2006) in which the structural and functional features of these two very similar looking pine leaves were investigated to gain an understanding of how nature evolved two very differently behaving structures. We now have a better understanding of how rather subtle variances in the internal anatomy of the pine needle can significantly influence its biophysical properties. Variation in patterns of cell wall thickening of the endodermis and degree of internal lignification appear to be key to these differences. Our finding that these different anatomical aspects lead to contrasting biophysical properties could have applications as far reaching as the engineering of structures, such as better controlling the physical properties of manufactured cables or sandwich composite materials.

LITERATURE CITED

- BEISMANN, H., H. WILHELMI, H. BAILLERES, H. C. SPATZ, A. BOGENRIEDER, AND T. SPECK. 2000. Brittleness of twig bases in the genus *Salix*: Fracture mechanics and ecological relevance. *Journal of Experimental Botany* 51: 617–633.
- GIBSON, L. J., M. F. ASHBY, AND K. E. EASTERLING. 1988. Structure and mechanics of the iris leaf. *Journal of Materials Science* 23: 3041–3048.
- HAMMAN, K. D., R. L. WILLIAMSON, E. D. STEFFLER, C. T. WRIGHT, J. R. HESS, AND P. A. PRYFOGLE. 2005. Structural analysis of wheat stems. *Applied Biochemistry and Biotechnology* 121: 71–80.
- HARDIN, J. W., D. J. LEOPOLD, AND F. M. WHITE. 2001. Textbook of dendrology. McGraw Hill, Boston, Massachusetts, USA.
- KAACK, K., AND K. SCHWARZ. 2001. Morphological and mechanical properties of *Miscanthus* in relation to harvesting, lodging, and growth conditions. *Industrial Crops and Products* 14: 145–154.
- KAACK, K., K. SCHWARZ, AND P. E. BRANDER. 2003. Variation in morphology, anatomy and chemistry of stems of *Miscanthus* genotypes differing in mechanical properties. *Industrial Crops and Products* 17: 131–142.
- KARAMANOS, S. A. 2002. Bending instabilities of elastic tubes. *International Journal of Solids and Structures* 39: 2059–2085.
- LEKHNITSKII, S. G. 1968. Anisotropic plates. In S. W. Tsai and T. Cheron [translators], 448. Gordon and Breach Science Publishers, New York, New York, USA.
- MILWICH, M., T. SPECK, O. SPECK, T. STEGMAIER, AND H. PLANCK. 2006. Biomimetics and technical textiles: Solving engineering problems with the help of nature's wisdom. *American Journal of Botany* 93: 1455–1465.
- MOULIA, B., AND M. FOURNIER. 1997. Mechanics of the maize leaf: A composite beam model of the midrib. *Journal of Materials Science* 32: 2771–2780.
- MOULIA, B., M. FOURNIER, AND D. GUITARD. 1994. Mechanics and form of the maize leaf: In-vivo qualification of flexural behavior. *Journal of Materials Science* 29: 2359–2366.
- NIKLAS, K. J. 1991. Bending stiffness of cylindrical plant organs with a 'core-rind' construction: Evidence from *Juncus effusus* leaves. *American Journal of Botany* 78: 561–568.
- NIKLAS, K. J. 1992. Plant biomechanics. University of Chicago Press, Chicago, Illinois, USA.
- RUZIN, S. E. 1999. Plant microtechnique and microscopy. Oxford University Press, New York, New York, USA.
- SPATZ, H. C., H. BEISMANN, F. BRÜCHERT, A. EMANNS, AND T. SPECK. 1997. Biomechanics of the giant reed *Arundo donax*. *Philosophical Transactions of the Royal Society of London, B, Biological Sciences* 352: 1–10.
- SPATZ, H. C., C. BOOMGAARDEN, AND T. SPECK. 1993. Contribution to the biomechanics of plants. 3. Experimental and theoretical studies of local buckling. *Botanica Acta* 106: 254–264.
- SPATZ, H. C., AND A. EMANNS. 2004. The mechanical role of the endodermis in *Equisetum* plant stems. *American Journal of Botany* 91: 1936–1938.
- SPATZ, H. C., L. KOEHLER, AND T. SPECK. 1998. Biomechanics and functional anatomy of hollow-stemmed sphenopsids. I. *Equisetum giganteum* (Equisetaceae). *American Journal of Botany* 85: 305–314.
- SPECK, T. O., A. EMANNS, AND H. C. SPATZ. 1998. Biomechanics and functional anatomy of hollow stemmed sphenopsids. III. *Equisetum hyemale*. *Botanica Acta* 111: 366–376.
- SPECK, T. O., AND H. C. SPATZ. 2003. Mechanical properties of the rhizome of *Arundo donax* L. *Plant Biology* 5: 661–669.
- VINCENT, J. F. V. 1982. The mechanical design of grass. *Journal of Materials Science* 17: 856–860.
- WANG, J., J. M. ZHU, Q. Q. LIN, X. J. LI, N. J. TENG, Z. S. LI, B. LI, A. M. ZHANG, AND J. X. LIN. 2006. Effects of stem structure and cell wall components on bending strength in wheat. *Chinese Science Bulletin* 51: 815–823.